Commun Nonlinear Sci Numer Simulat 22 (2015) 731–746

Contents lists available at ScienceDirect

Commun Nonlinear Sci Numer Simulat

journal homepage: www.elsevier.com/locate/cnsns

Circular, elliptic and oval billiards in a gravitational field

Diogo Ricardo da Costa [a,b,c,*], Carl P. Dettmann [b], Edson D. Leonel [c,d]

[a] Instituto de Física da USP, Rua do Matão, Travessa R 187, Cidade Universitária, 05508-090 São Paulo, SP, Brazil
[b] School of Mathematics, University of Bristol, Bristol, United Kingdom
[c] Departamento de Física, UNESP – Univ Estadual Paulista, Av.24A, 1515, 13506-900 Rio Claro, SP, Brazil
[d] The Abdus Salam, ICTP, Strada Costiera, 11, 34151 Trieste, Italy

ARTICLE INFO

Article history:
Received 19 October 2013
Received in revised form 20 August 2014
Accepted 24 August 2014
Available online 3 September 2014

Keywords:
Circular
Elliptic
Oval
Billiard
Gravitational field

ABSTRACT

We consider classical dynamical properties of a particle in a constant gravitational force and making specular reflections with circular, elliptic or oval boundaries. The model and collision map are described and a detailed study of the energy regimes is made. The linear stability of fixed points is studied, yielding exact analytical expressions for parameter values at which a period-doubling bifurcation occurs. The dynamics is apparently ergodic at certain energies in all three models, in contrast to the regularity of the circular and elliptic billiard dynamics in the field-free case. This finding is confirmed using a sensitive test involving Lyapunov weighted dynamics. In the last part of the paper a time dependence is introduced in the billiard boundary, where it is shown that for the circular billiard the average velocity saturates for zero gravitational force but in the presence of gravitational it increases with a very slow growth rate, which may be explained using Arnold diffusion. For the oval billiard, where chaos is present in the static case, the particle has an unlimited velocity growth with an exponent of approximately 1/6.

1. Introduction

In the 1920s billiards were introduced by Birkhoff [1] into the theory of dynamical systems. They consist of a point particle moving freely in a region except for specular collisions with the boundary. Birkhoff's idea was to have a simple class of models which shows the complicated behavior of non-integrable smooth Hamiltonian systems without the need to integrate a differential equation [1,2]. Depending on the shape of the boundary, billiard dynamics may be (i) regular, with only periodic or quasi-periodic orbits present; (ii) mixed, in which chaos, KAM islands (also called periodic islands) and invariant spanning curves that limit the chaos in the systems are present; (iii) completely ergodic, presenting only chaos in the phase space.

In recent years billiards continue to provide useful models for Hamiltonian dynamics, as well as problems involving free motion in cavities and in extended structures. The latter includes the study of anomalous diffusion in geometries with infinite horizon [3–5]. Mixed phase space models include mushroom billiards [6,7]. Time irreversible billiards have also been considered [8] as well as connections with many wave and quantum mechanical problems [9–12]. Further examples are reviewed in [13].

It can be useful to open the billiard geometry by including a hole and investigating escape time and related distributions. Open billiards provide a useful starting point for an understanding of more general classes of open dynamical systems [13]

* Corresponding author at: Instituto de Física da USP, Rua do Matão, Travessa R 187, Cidade Universitária, 05508-090 São Paulo, SP, Brazil.
E-mail address: diogo_cost@hotmail.com (D.R. da Costa).

http://dx.doi.org/10.1016/j.cnsns.2014.08.030
1007-5704/

and include the study of open circular billiards and the Riemann hypothesis [14]. Sometimes it is useful to investigate the survival probability or the histogram of particles that reached certain height in the phase space [15].

An important subject in this area is the study of Fermi acceleration (FA) [16]. The phenomenon is characterized by an unlimited energy growth of a bouncing particle undergoing collisions with a periodically moving and heavy wall. According to the Loskutov–Ryabov–Akinshin (LRA) conjecture [17], the introduction of a time dependence to the boundary of a billiard is a sufficient condition to observe FA when the corresponding static billiard has chaotic components. The elliptical case however must be treated separately and the LRA conjecture does not apply for it. For the static boundary it is integrable and hence has a phase space showing only regular structures. There are two quantities which are preserved in the elliptical billiard with static boundary: (i) energy (E) and; (ii) product of the angular momenta about the two foci (F) as discussed in [18]. However, it was shown recently [19] that the introduction of a periodically time perturbation to the boundary does lead to FA. The explanation for observing diffusion in velocity is mainly related to the existence of a separatrix in the phase space. According to [19], after introducing a time perturbation to the boundary, the separatrix turns into a stochastic layer yielding a type of turbulent behavior in F therefore leading to diffusion in velocity, hence producing the FA. More simulations were done in the model [20] which confirmed the FA. Due to this observation in the elliptical billiard and considering the LRA conjecture, a recent work [21] argues that the existence of heteroclinic fixed point in the phase space may extend the conjecture in the absence of chaos in the phase space. The circular billiard does not have such a fixed point and remains regular even with vibrating boundaries. Even in [21], the authors claim that FA seems not to be a robust phenomena. The reflection law may be modified so that the particle experiences a slightly inelastic collision therefore having a fractional loss of energy upon collision. Even in such a small limit of dissipation, the unlimited energy growth is suppressed.

It is also interesting to study billiards in the presence of a constant gravitational field. The Galton board (1873) is a mechanical device that exhibits stochastic behavior. It consists of a vertical (or inclined) board with interleaved rows of pegs, where a ball moving into the Galton board moves under gravitation and bounces off the pegs on its way down [22]. There have been many recent investigations in gravitational billiards including a physical experiment observing stable islands in chaotic atom-optics billiards [23], characterization of the dynamics of a dissipative, inelastic gravitational billiard [24], the study of linear stability in billiards with potential [2] and many others [25–28]. It also includes the wedge billiard [24,29–31] which has singular regions in the phase space that cannot be described by the KAM theorem [26]. In Ref. [2] it is discussed the way to obtain the linear stability of billiards with potentials for which the free motion is integrable. Examples include the linear gravitational potential, the constant magnetic field, the harmonic potential, and a billiard in a rotating frame of reference, imitating the restricted three-body problem [2].

The purpose of the present paper is to investigate some gravitational convex billiards, with or without vibrating boundaries. As noted above, the static and vibrating circular billiards and static elliptical billiards have regular dynamics in the absence of a gravitational field, while oval and vibrating elliptical billiards usually have mixed phase space. We apply the approach in Ref. [2] to characterize linear stability of fixed points in the presence of the external field exactly in terms of the curvature of the boundary and normal component of the velocity at the point(s) of collision. A numerical search identifies apparently ergodic energy values, even for the circular billiard; we then apply a sensitive Lyapunov weighted dynamics test to further confirm this [32]. As mentioned in the work of Tailleur and Kurchan [32], this method was proposed and adapted from the context of chemical reactions [33–35]. They have demonstrated that their method is capable of finding even very small stability regions in systems of many degrees of freedom [36]. Ergodicity is interesting as it may suggest the existence of a new class of ergodic billiards, extending known results for dispersing and defocusing non-gravitational billiards on one hand and for the gravitational but piecewise linear wedge billiard on the other. In non-gravitational billiards it is known that no smooth convex billiard can be ergodic [37,38].

Finally, we introduce a time-dependence in the billiard, and show for the circle in the absence of gravitational field and as expected, the average velocity of the system approaches a regime of saturation. In the presence of gravitational field, the velocity keeps growing for long number of collisions but with a small slope of growth, an interesting effect since in the high velocity limit the gravitational field has less and less effect, so the dynamics approaches the non-gravitational regular behavior. We can explain the continued but slow acceleration in terms of Arnold diffusion. For the breathing oval billiard, our numerical result for the slope of growth is slightly larger than the one obtained in the [39] and theoretically foreseen in [40] but still of the same order of magnitude.

This paper is organized as follows: in the Section 2 we describe the model and obtain the mapping that describes the dynamical of a particle. In Section 3 we study the energy regimes and explore the phase space for different values of the control parameters. Section 4 is devoted to study some periodic orbits, for the oval, ellipse and consider the low energy regime. Apparent ergodicity is studied in the Section 5. In Section 6 we take into account the time-dependent billiards. Our conclusions and final remarks are presented in 7.

2. The model and the map

The models we are considering consist of a classical particle (or an ensemble of non-interacting particles) confined inside and experiencing collisions with a closed boundary of circular, elliptic and oval shapes under the presence of a gravitational force. To describe the dynamics, we follow the same general procedure as made in [39]. Then the dynamics of each particle is described in terms of a four-dimensional nonlinear mapping $T(\theta_n, \alpha_n, |\overrightarrow{V}_n|, t_n) = (\theta_{n+1}, \alpha_{n+1}, |\overrightarrow{V}_{n+1}|, t_{n+1})$ where the variables

denote: (θ) the angular position of the particle; (α) the angle that the trajectory of the particle forms with the tangent line at the position of the collision; $(|\vec{V}|)$ the absolute velocity of the particle and; (t) the instant of the collision with the boundary. The shape of the boundary is defined by its corresponding radius in polar coordinates which is given by

$$R(\theta, p, \epsilon) = 1 + \epsilon \cos(p\theta), \tag{1}$$

where $\epsilon \in [0, 1)$ is a parameter which controls the deformation of the boundary (see for example [18]) and p is a positive integer number. For $\epsilon = 0$ the circular billiard is recovered. In the Fig. 1 we have a sketch of the boundary and angles considering $p = 2$ and $\epsilon = 0.3$ (oval billiard). As one can see we have locally negative curvatures in $\theta = \pi/2$ and $\theta = 3\pi/2$. The radius of the elliptic billiard is given by the following expression (see also [19–21])

$$R(\theta, a, b) = \frac{ab}{\sqrt{(b\cos\theta)^2 + (a\sin\theta)^2}}, \tag{2}$$

where a and b are one-half of the ellipse's major and minor axes. If $a = b > 0$ the circular billiard is observed.

The rectangular components of the boundary at position (θ_n) are given by

$$X(\theta_n) = R(\theta_n)\cos(\theta_n), \tag{3}$$

$$Y(\theta_n) = R(\theta_n)\sin(\theta_n). \tag{4}$$

Starting with an initial condition $(\theta_n, \alpha_n, |V_n|, t_n)$, the angle between the tangent at the boundary and the horizontal axis at the point $X(\theta_n)$ and $Y(\theta_n)$ is given by $\phi_n = \arctan[Y'(\theta_n)/X'(\theta_n)]$, where

$$X' = dX/d\theta \quad \text{and} \quad Y' = dY/d\theta. \tag{5}$$

Since there is a gravitational force acting on the particle during the flight, its trajectory is described by arcs of parabolas. For $t > t_n$ the position of the particle as a function of time is given by

$$X_p(t) = X(\theta_n) + |\vec{V}_n|\cos(\alpha_n + \phi_n)(t - t_n), \tag{6}$$

$$Y_p(t) = Y(\theta_n) + |\vec{V}_n|\sin(\alpha_n + \phi_n)(t - t_n) - \frac{g(t - t_n)^2}{2}. \tag{7}$$

Once the position of the particle as a function of the time is known, its distance measured with respect to the origin of the coordinate system is given by $R_p(\theta_p, t) = \sqrt{X_p^2(t) + Y_p^2(t)}$ and θ_p at $(X_p(t), Y_p(t))$ is $\theta_p = \arctan[Y_p(t)/X_p(t)]$. The angular position at the next collision of the particle with the boundary, i.e. θ_{n+1}, is numerically obtained by solving the following equation $R(\theta, t) = R_p(\theta, t)$. The time is obtained by

$$t_{n+1} = t_n + \frac{\sqrt{\Delta X^2 + \Delta Y^2}}{|\vec{V}_n|}, \tag{8}$$

where $\Delta X = X(\theta_{n+1}) - X(\theta_n)$ and $\Delta Y = Y(\theta_{n+1}) - Y(\theta_n)$. At the instant of collision, we use the following reflection law

$$\vec{V}'_{n+1} \cdot \vec{T}_{n+1} = \vec{V}'_n \cdot \vec{T}_{n+1}, \tag{9}$$

$$\vec{V}'_{n+1} \cdot \vec{N}_{n+1} = -\vec{V}'_n \cdot \vec{N}_{n+1}, \tag{10}$$

where $\vec{T}$ and $\vec{N}$ are the unit tangent and normal vectors and $\vec{V}'$ denotes the velocity of the particle measured in the moving referential frame. Based on these two last equations, the particle's velocity components after collisions are given by

$$\vec{V}_{n+1} \cdot \vec{T}_{n+1} = V_x\cos(\phi_{n+1}) + V_y\sin(\phi_{n+1}),$$
$$\vec{V}_{n+1} \cdot \vec{N}_{n+1} = V_x\sin(\phi_{n+1}) - V_y\cos(\phi_{n+1}),$$

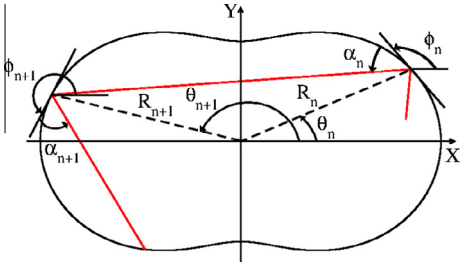

Fig. 1. Sketch of the boundary and angles considering $p = 2$ and $\epsilon = 0.3$ (oval billiard). As one can see we have locally negative curvatures in $\theta = \pi/2$ and $\theta = 3\pi/2$.

where

$$V_x = |\vec{V}_n|\cos(\alpha_n + \phi_n),$$
$$V_y = |\vec{V}_n|\sin(\alpha_n + \phi_n) - g(t_{n+1} - t_n).$$

Therefore, the velocity of the particle at collision $(n+1)$ is given by

$$|\vec{V}_{n+1}| = \sqrt{(\vec{V}_{n+1}\cdot\vec{T}_{n+1})^2 + (\vec{V}_{n+1}\cdot\vec{N}_{n+1})^2}. \tag{11}$$

Finally, α_{n+1} is obtained as

$$\alpha_{n+1} = \arctan\left[\frac{\vec{V}_{n+1}\cdot\vec{N}_{n+1}}{\vec{V}_{n+1}\cdot\vec{T}_{n+1}}\right]. \tag{12}$$

3. Energy regimes

In this section we present our numerical results for the circular, elliptic and oval billiards. To construct the phase space of the systems, it is essential to note the conserved energy $E = K + U$, where $K = mV^2/2$ is the kinetic energy of the particle. The potential energy is given by $U = mgh$, where h is the height of the particle measured with respect to an arbitrary reference and m is the mass of the particle considered as unitary in our simulations. Eq. (1) has as its origin the center of the circle/oval billiard, but we consider as a reference level the bottom of the billiard. Therefore the reference level for the gravitational energy is obtained applying $Y \to Y + Y_{ref}$, where Y_{ref} is used to translate the vertical axis and is given by $Y_{ref} = R(\theta = \pi/2)\sin(p\pi/2) = 1 + \epsilon\cos(p\pi/2)$. Hence the potential energy of a particle is given by $U = g(Y(\theta) + Y_{ref})$, leading to

$$U(p, \epsilon, \theta, g) = g\sin(\theta)[1 + \epsilon\cos(p\theta)] + 1 + \epsilon\cos(p\pi/2). \tag{13}$$

For the elliptic billiard we have that $Y_{ref} = R(\theta = \pi/2) = b$. Setting the energy constant, we write the initial velocity as

$$V_0 = \sqrt{2[E - U(\theta_0)]}. \tag{14}$$

If $E = 0$ the particle does not have enough energy to leave the bottom of the billiard, then we consider $E > 0$.

Having constructed the collision map and incorporated energy conservation, let us now investigate the dynamics looking at the phase space. We start with the circular billiard, which can be obtained considering $\epsilon = 0$ in Eq. (1) or $a = b > 0$ in Eq. (2). Fig. 2(a) shows a phase space for the circular billiard considering the energy $E = 2$ and $g = 0.5$.

Each of the phase space shown in the figure was constructed considering a grid of 10 by 10 equally spaced initial conditions in the intervals $\theta_0 \in [0, 2\pi)$ and $\alpha_0 \in [0, \pi)$, where the initial velocity is given by Eq. (14) and $t_0 = 0$. Each initial condition was iterated up to 2000 collisions with the boundary. For $E = 2$ and $g = 0.5$, as shown in Fig. 2(a), we see two islands around $\theta = \pi/2$ and $\theta = 3\pi/2$ (for $\alpha = \pi/2$), defining a period two periodic orbit in the center. In the limit of $E \to \infty$ the velocity of the particle increases and the arcs of parabola describing the motion of the particle become straight lines. The phase space for the circular billiard in the absence of gravitational field billiard is recovered, and only periodic and quasi-periodic obits are observed. When considering $E = 2$ in Fig. 2(a), we observed that this energy is too high and the gravitational field does not affect the dynamics significantly. After decreasing the energy, it was observed several inverse and direct parabolic bifurcations, as well as the creation of chaotic regions due to the raise of instability through resonances. But for $E \to 0$ no chaotic orbits are observed, and only regular and quasi-regular orbits can be seen in the system.

Considering $E = 1.416$ as shown in Fig. 2(b) we see that the phase space is of mixed type. Now changing the energy to $E = 1.088$, we see the fixed points in $\theta = \pi/2$ or $\theta = 3\pi/2$ become unstable, creating a period four elliptic periodic orbit. For $E = 0.72$ (see Fig. 2(d)) KAM islands are not observed and an apparent ergodic region emerges. More details are shown later.

Decreasing the energy to $E = 0.3$ (see Fig. 2(e)) the chaotic sea occupies a small region of the phase space and some KAM islands are now visible. Decreasing yet more the energy to $E = 0.1$ (Fig. 2(f)) we see that periodic (or quasi periodic) orbits are present and chaos is no longer present. The fixed point in $\theta = 3\pi/2$ is stable (elliptical). More details about the change of stability of the fixed points are shown in the Section 4.

Let us study the phase space for a convex oval billiard considering $\epsilon = 0.1$ and $p = 2$. In Fig. 3(a) we see a phase space for $g = 0$ (absence of gravitational field). The phase space is then of mixed type. Another way to obtain Fig. 3(a) for $g = 0.5$ is to consider the energy $E \to \infty$. In Fig. 3(b) $g = 0.5$ for a constant energy $E = 1$ while fixed point in $\theta = \pi/2$ and $3\pi/2$ becomes unstable and creates a period four elliptical fixed point. Considering $E = 0.8$ and for fixed value of $g = 0.5$ we observe in Fig. 3(c), there is a region where the orbits cannot access. This happens because of the energy conservation and the particle does not have enough energy to reach such regions. Fig. 3(d), with $E = 0.651256$, shows a phase space where KAM islands are not observed. Decreasing the value of energy to $E = 0.3$ (see Fig. 3(e)) the chaotic sea is confined in a small region of the phase space. Changing the energy to $E = 0.1$ (Fig. 3(f)) we see only periodic (or quasi periodic) orbits are observed and chaos is no longer present, as similar to Fig. 2(a).

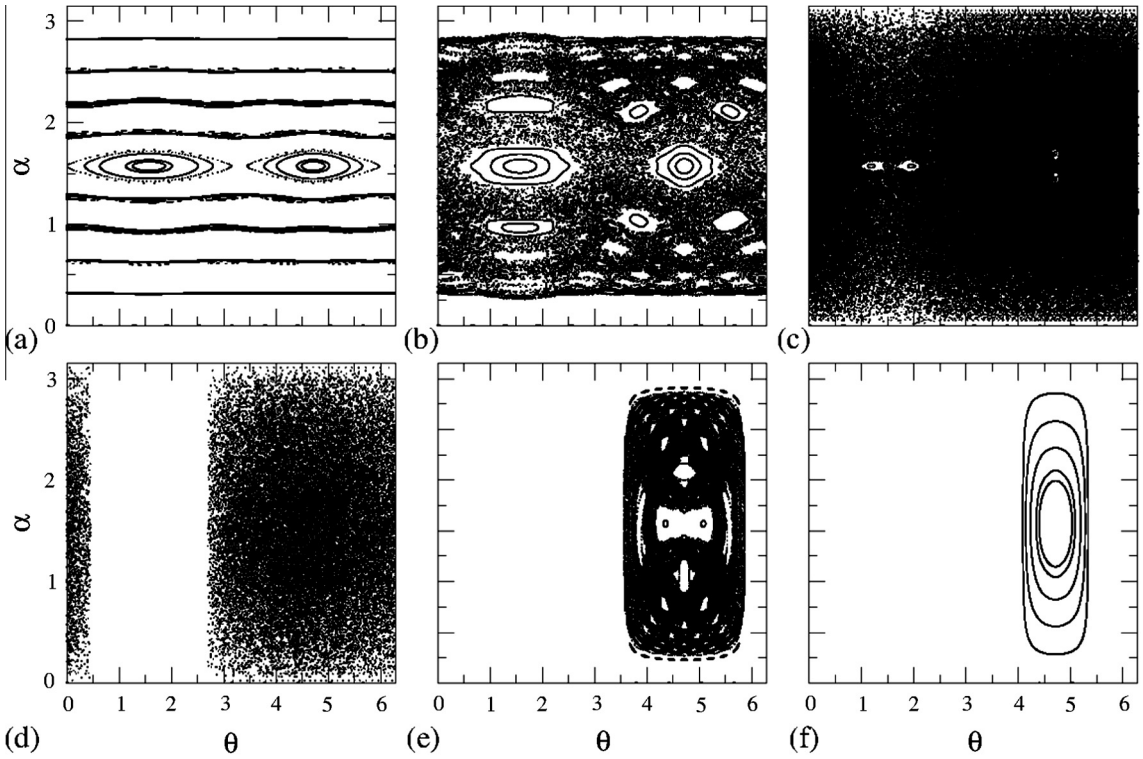

Fig. 2. Phase space for the circle ($\epsilon = 0$) with $g = 0.5$, considering: (a) $E = 2$; (b) $E = 1.416$; (c) $E = 1.088$; (d) $E = 0.72$; (e) $E = 0.3$; (f) $E = 0.1$.

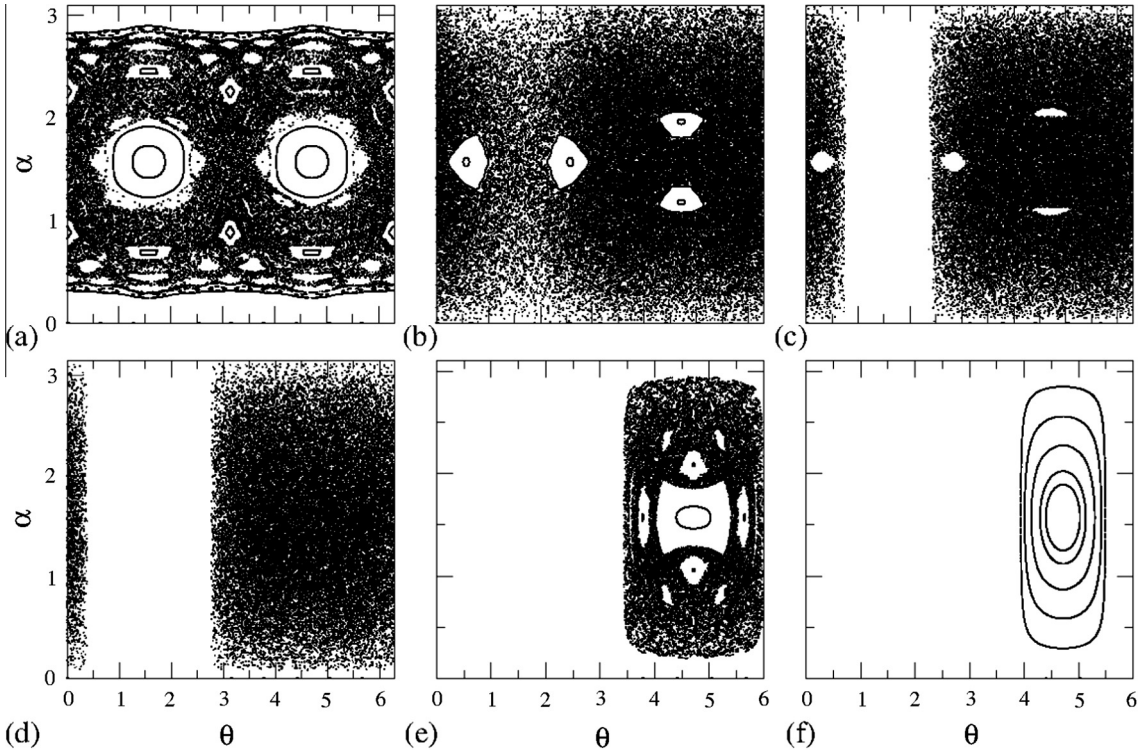

Fig. 3. Phase space for a convex oval billiard ($p = 2$ and $\epsilon = 0.1$). In (a) $g = 0$. For $g = 0.5$ we have: (b) $E = 1$; (c) $E = 0.8$; (d) $E = 0.651256$; (e) $E = 0.3$; (f) $E = 0.1$.

Results for the elliptic billiard are shown in Fig. 4. The control parameters used in the simulations were $a = 1.2, b = 1$ and $g = 0.5$. Fig. 4(a) shows the phase space considering $E = 4$. As one can see the chaotic sea is observed near $\alpha \cong \pi/2$, and periodic or quasi periodic regions can be observed above and below such α. For $E \to \infty$ only periodic or quasi-periodic orbits are observed, therefore the results for the absence of gravitational field are recovered. Of course this case can also be obtained considering $g = 0$. The fixed points in $\theta = \pi/2$ and $\theta = 3\pi/2$ (for $\alpha = \pi/2$) are elliptical (stable). Decreasing the value of the energy for $E = 1.288$ produces a phase space where a saddle fixed point can be observed in $\theta = \pi/2$ and $\theta = 3\pi/2$, as shown in Fig. 4(b). Decreasing even more the energy turns the fixed point unstable (hyperbolic fixed point). The phase space for $E = 0.94$ is shown in Fig. 4(c), and as one can see the fixed point in $\theta = \pi/2$ is no longer available. Again there is a forbidden region that appears due to the conservation of energy. For $E = 0.824$ the phase space is apparently ergodic (see Fig. 4(d)). Fig. 4(e) shows the chaotic sea is observed in a small region of the phase space, and the number of KAM islands is quite large. Finally, in the limit $E \to 0$ the phase space presents periodic and quasi-periodic regions, as shown in Fig. 4(f) considering $E = 0.1$, again similar to the previous cases.

To conclude, we see that the phase space for the circle, elliptic and oval billiards have some common characteristics: all of them present apparent ergodic regions for some combinations of control parameters; for $E \to 0$ the chaotic sea tends to disappear; these systems present changes of stability for the fixed points in $\theta = \pi/2$ or $\theta = 3\pi/2$ ($\alpha = \pi/2$). However, despite of the similarities pointed here, there are also marked differences.

3.1. Supplemental data I

As attached files we have three different videos showing details about the phase spaces of Figs. 2–4. For all, we have considered $g = 0.5$ and the energy is varied in the interval $E \in (0, 2)$. The phase space α vs θ for the circle, oval and elliptic billiards can be found in the following addresses: http://youtube.com/watch?v=Brb3GHXjfFE, http://youtube.com/watch?v=heWA0HPJcGQ and http://youtube.com/watch?v=BM4oSeXTGxk. To construct the frames, we used a grid of 500 by 500 different initial conditions and each orbit was iterated up to 2000 times. As we can see there exist a lot of duplication of periods and a complicated behavior can be observed.

4. Periodic orbits

In this section we concentrate to study the linear stability of some periodic orbits in the phase space. We start investigating what happens with the fixed points $\theta = \pi/2$ and $\theta = 3\pi/2$ (for $\alpha = \pi/2$) in Figs. 2(b,c) or 3(a,b). In them we see

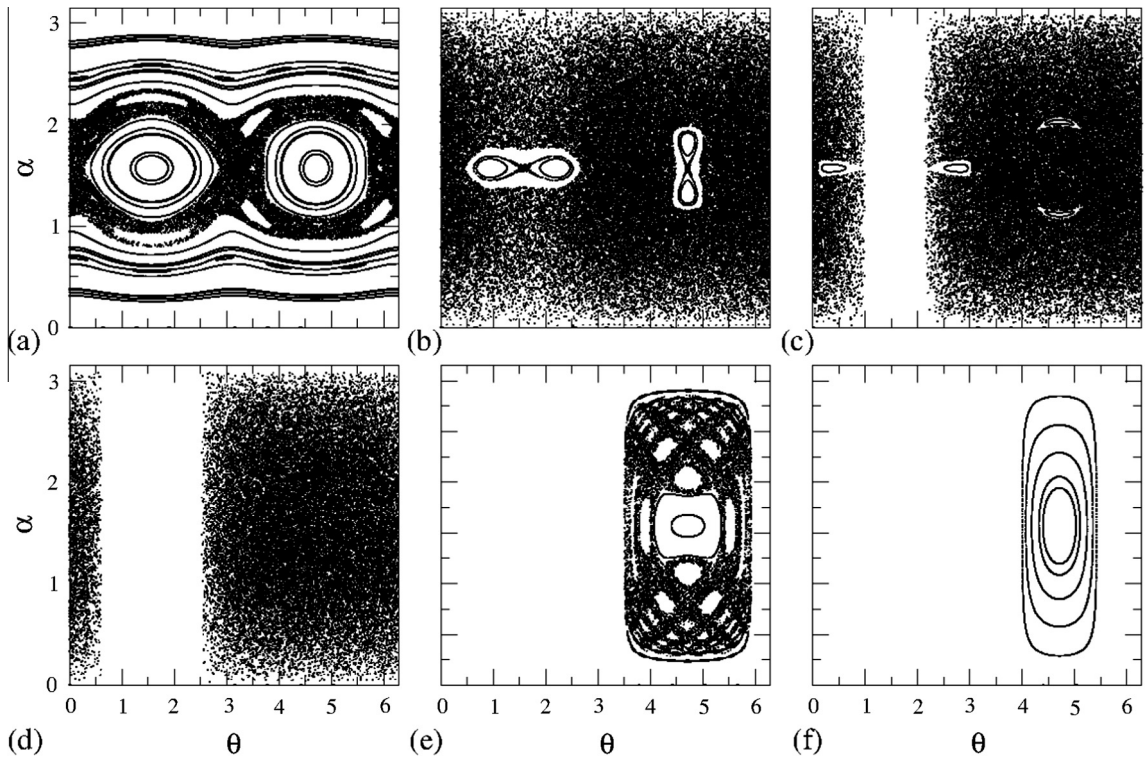

Fig. 4. Phase space for an elliptic billiard ($a = 1.2, b = 1.0$ and $g = 0.5$) considering: (a) $E = 4$; (b) $E = 1.28$; (c) $E = 0.94$; (d) $E = 0.824$; (e) $E = 0.3$; (f) $E = 0.1$.

the left fixed point ($\theta = \pi/2$ and $\alpha = \pi/2$) in the Figs. 2(b,c) and 3(a) is elliptical and after decreasing the energy (Figs. 2(c) and 3(b)), it becomes unstable and a period four fixed point arises. The duplications in the left occur in the horizontal axis and in the right occurs in the vertical. It happens this way because the trajectories are arcs of parabola for $g > 0$ and as can be seen in Fig. 5(b) it needs to hit another part (by looking at two separate parts measured with respect to an imaginary line cutting/separating the billiard at $x = 0$) of the billiard to continue in a periodic orbit. This behavior is different for $g = 0$ or $E \to \infty$, where the fixed point hits the top and bottom of the billiard (see Fig. 5(a)). Another way to observe the phenomenon in Fig. 3(a,b) is to consider initially $g = 0$ and increasing it until the fixed point becomes unstable.

The position (θ, α) of the elliptical fixed points in $\theta \cong \pi/2$ and $\theta \cong 3\pi/2$ (for $\alpha = \pi/2$) can be obtained numerically. Therefore it is possible to find the critical value of g in which there is a change from stable to unstable (saddle) fixed point denoted as g_c. We then obtain a period-doubling bifurcation. For the oval billiard, we have in Fig. 6(a) g_c/E as function of the control parameter ϵ and using four different values of E. We rescaled the vertical axis by E because it is proportional to g. Then g_c/E is a constant as can be seen in Fig. 6(a) looking at the fact that for different values of E, the curve has an universal behavior. Therefore, these curves of g_c/E as function of ϵ are scaling invariant for E. Under this curve, the fixed point in $\alpha = \pi/2$ and $\theta = \pi/2$ (or $\theta = 3\pi/2$) is elliptical and above this, it is unstable (hyperbolic).

Similar analysis can be done in the elliptic billiard. The results of g_c/E as function of the control parameter a for different values of energy are shown in Fig. 6(b) for $b = 1$. The curves are again scaling invariant for E.

The behavior of the fixed points can be obtained analyzing the linear stability. To compute this it is convenient to introduce Green's residue R and its complement $\bar{R}$, which are defined by $\bar{R} = 1 - R = \ \mathrm{tr}^{(4)}/4 = (2 + \ \mathrm{tr})/4$,where $\mathrm{tr}_j^{(4)} = \ \mathrm{tr}\prod_{i=1}^{j}\mathbf{M}_i^{(4)}\mathbf{K}_i^{(4)}$. $\mathbf{K}^{(4)}$ is the linearized reflection matrix. The stability is split up into contributions from the reflection $\mathbf{K}^{(4)}$ and from the free motion $\mathbf{M}^{(4)}$. j is the period of the orbit. More details can be obtained in the Ref. [2].

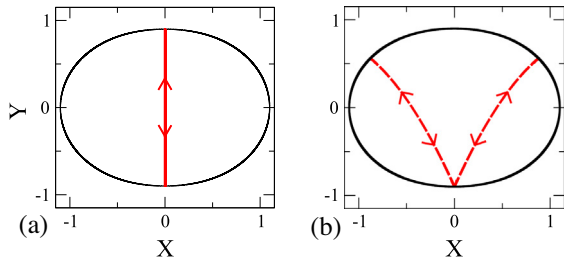

Fig. 5. For the oval billiard with $p = 2$ and $\epsilon = 0.1$ we have in (a) the trajectory for an elliptic fixed point in $\theta = \pi/2$ or $\theta = 3\pi/2$ ($\alpha = \pi/2$) when considering $g = 0$. As one can see the particle bounces between the top and bottom parts of the billiard. In (b), for $g = 0.5$ and $E = 1$, we can an example of trajectory after the bifurcation, with the creation of a period four fixed point.

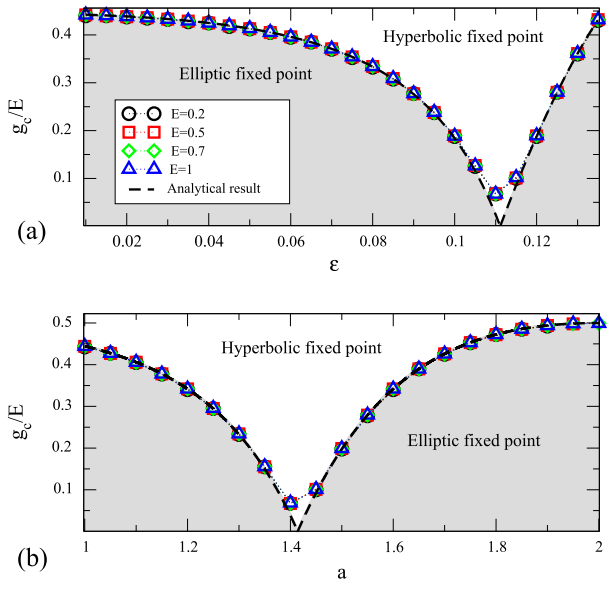

Fig. 6. For $t_0 = 0, \theta_0 = \pi/2 + 10^{-8}$ and $\alpha_0 = \pi/2$ we have the numerical and analytical results for: (a) g_c/Evs$\epsilon \in [0.01, 0.135]$ for the oval billiard with $p = 2$ and considering four different values of energy E; (b) g_c/E vs $a \in [1, 2]$ for the elliptic billiard with $b = 1$.

We use the following formulae to calculate the Residue of symmetric orbits:

$$R = 4R'(1-R') \quad \bar{R} = \left(1-2\bar{R}'\right)^2. \tag{15}$$

For the fixed points mentioned in Fig. 3(a), i.e., orbits that touch the top and bottom of the billiard, we show the residue for $\alpha = \pi/2$ and $\theta = \pi/2$ (or $\theta = 3\pi/2$) is equal to [2]

$$R' = 1 - V^*\kappa\tau', \tag{16}$$

where $\tau' = \tau/2$ and τ is the time spend for the particle to return to the initial point. V^* is the normal component of the velocity and κ is the curvature in the collision point. It is important to say that if $0 < R < 1$ the fixed point is elliptical.

For $E > 2g(1-\epsilon)$ we ensure the particle touches the top and bottom of the billiard (see Fig. 5(a)). The time τ' for the particle to travel the distance between the top and bottom (or vice versa) is equal to

$$\tau' = \frac{V_d - V_u}{g}. \tag{17}$$

Here $V_d = \sqrt{2E}$ and $V_u = \sqrt{2E - 4gR(\theta = \pi/2)}$ are the velocities, respectively, in the bottom part (where the potential energy U is equal to zero) and in the upper part of the billiard.

For billiards, the curvature κ can be obtained using the following expression (see for example [41])

$$\kappa(\theta) = \frac{X'(\theta)Y''(\theta) - X''Y'(\theta)}{\left[X'^2(\theta) + Y'^2(\theta)\right]^{3/2}}, \tag{18}$$

where $X'' = d(X')/d\theta$ and $Y'' = d(Y')/d\theta$ (X' and Y') were previously defined in Eq. (5).

In order to better present the analytical and numerical results, we separate the findings in two different parts. First we analyze the oval/circle billiards and after that the results for the elliptic billiard are obtained.

4.1. Oval

For the oval billiard, when considering $\theta = \pi/2$ or $\theta = 3\pi/2$, the curvature, using the Eq. (18), is written as

$$\kappa = \frac{R\left[R - R''^2\right] + 2R'^2}{\left(R^2 + R''^2\right)^{3/2}}. \tag{19}$$

In this case $R = R(\theta = \pi/2)$, $R' = \frac{\partial R}{\partial\theta}(\theta = \pi/2)$ and $R'' = \frac{\partial R'}{\partial\theta}(\theta = \pi/2)$.

After obtaining R' in Eq. (16), we can evaluate R in Eq. (15). Considering $R = 0$ and $V^* = V_u$, we show that g_c is given by

$$g_c = -E\frac{4\kappa[1 + 2\kappa(\epsilon - 1)]}{[1 + 4\kappa(\epsilon - 1)]^2}, \tag{20}$$

where κ is given by Eq. (19). As one sees from previous equation, E is scaling invariant. If we define a new variable g/E the result obtained for different E are basically the same, confirming the rescaling made in Fig. 6(a).

Now considering $R = 0$ and $V^* = V_d$, we found that g_c/E is written as

$$\frac{g_c}{E} = 2\kappa - 4\kappa^2(\epsilon - 1) + 2\kappa[1 + 2(\epsilon - 1)]. \tag{21}$$

We need to find the condition in which Eqs. (20) and (21) have the same values, and the value of g when it happens is given by

$$g^* = \frac{1}{2}\frac{(2\kappa - 1)}{\kappa}. \tag{22}$$

According to our results, Eq. (20) fits the numerical results for $g < g^*$, and Eq. (21) is used when $g > g^*$. The results here are general, applying to every control parameter g, E, ϵ and p of the oval billiard.

For a particular case, with $p = 2$ (convex oval billiard) we have that the curvature is equal to

$$\kappa(\epsilon) = \frac{(1 - 5\epsilon)}{(1 - \epsilon)^2}. \tag{23}$$

In this situation, we value of g^* is equal to $1/9$ (see Eq. (22)). The results for $\epsilon < 1/9$ in Fig. 6(a) can be obtained considering $R = 0$ and $V^* = V_u$. As result we obtain analytically a curve for g_c as function of ϵ which is equal to

$$g_c = E\frac{(5\epsilon - 1)}{(19\epsilon - 3)(\epsilon - 1)}\left[\frac{a_1\left(a_2\epsilon - a_3 + |1 - 9\epsilon|\sqrt{2}\right)}{19\epsilon - 3} - 2\right], \tag{24}$$

where $a_1 = \sqrt{2}, a_2 = 10a_1$ and $a_3 = a_2/5$. For $\epsilon = 0$ (circle billiard), the value of g_c is equal to 4/9. For $\epsilon > g^* = 1/9$, it is necessary to consider $V^* = V_d$ and $R = 0$, and the result obtained is

$$g_c = E\frac{(5\epsilon - 1)}{(\epsilon - 1)^2}\left[\frac{a_1\left(a_2\epsilon - a_3 + |1 - 9\epsilon|\sqrt{2}\right)}{\epsilon - 1} - 2\right]. \tag{25}$$

As one can see for both cases dividing both sides of the equations for E yields g_c/E , which is a function of ϵ, therefore confirming the results shown in Fig. 6(a). Moreover the critical value of g is scaling invariant for the energy E. The analytical results obtained can be observed in Fig. 6(a) as the black dashed curves. As one can see, the numerical and analytical results are in good agreement.

4.2. Ellipse

Considering the elliptic billiard with radius given by Eq. (2), the curvature for $\theta = \pi/2$ or $\theta = 3\pi/2$ is given by

$$\kappa = \frac{b}{a^2}. \tag{26}$$

First of all we solve $R = 0$ considering $V^* = V_d$. After some calculations, the result obtained is

$$\frac{g}{E} = -\frac{2b}{a^4}\left(a^2 - 2b^2 + \left|a^2 - 2b^2\right|\right). \tag{27}$$

The solution of $R = 0$ and considering $V^* = V_u$ is given by

$$\frac{g}{E} = \frac{2b\left(2b^2 - a^2 + \left|a^2 - 2b^2\right|\right)}{\left(a^2 - 4b^2\right)^2}. \tag{28}$$

Combining Eqs. (28) and (27) we have

$$a = \sqrt{2}b. \tag{29}$$

After analyzing either the numerical and analytical results, we observe that Eqs. (27) and (28) are used for $a > \sqrt{2}b$ and $a < \sqrt{2}b$, respectively. These analytical results are confirmed in Fig. 6(b) as the black dashed lines, where the analytical and numerical results are in good agreement. For the situation shown in Fig. 6(b), with $b = 1$, we see that the minimum value of g_c/E is $\sqrt{2}$ (see Eq. (29)). As known, for $a = b = 1$, we have a circle with unitary radius. Considering Eq. (28), we show that $g_c/E = 4/9$. This is the same result obtained when considering $\epsilon = 0$ in the oval billiard.

It is interesting to see that the eccentricity of a ellipse is defined as $\sqrt{1 - (b/a)^2}$, therefore $g_c = 0$ when the eccentricity is 1/2.

4.3. Low energy

The results previously described cannot be applied to orbits that start in $\theta = 3\pi/2$ ($\alpha = \pi/2$) and do not reach the top boundary of the billiard. As example Fig. 9(a) shows a period one orbit with $g = 0.5, p = 2, \epsilon = 0.1$ and $E = 0.38$. It happens for orbits with $E < 2gR(\theta = \pi/2)$, where a period one fixed point is present. One can observe that the fixed point in $(\theta, \alpha) = (3\pi/2, \pi/2)$ is elliptical in Figs. 2(f) and 3(e,f), where E is a small value. Increasing E, the stable period one fixed point undergoes an inverse parabolic transition creating an elliptic period two orbit in a period doubling bifurcation, as shown in Figs. 2(e) and 3(d). Another example of such a bifurcation is shown in Fig. 9(b), for $g = 0.5, p = 2, \sigma = 0.1$ and $E = 0.416$, where a period two fixed point does not touch the top of the billiard. It happens because for focusing boundaries the orbit is elliptic for small energies and becomes inverse hyperbolic if the energy becomes large compared with the radius of curvature.

For the oval billiard, a good method to detect the bifurcation is to follow the position of the fixed points when varying E from 0 to $2gR(\theta = \pi/2)$. We call E_c as the energy in which the first period-doubling bifurcation is observed. In Fig. 7(a) we have E_c as function of g for $\epsilon = 0.01$ and $p = 2$, and after a linear fit we observe that $E_c = 0.51243g$ ($E_c \propto g$). E_c can be obtained by varying ϵ (consequently the curvature κ, which is given by Eq. (23)). It was done in Fig. 7(b) using $g = 0.1$. After fitting with a non-linear curve we obtained $E_c = 0.05026/\kappa$ ($E_c \propto 1/\kappa$). We conclude that $E_c \propto g/\kappa$. Such result can be proved analytically if one consider that $\tau = 2V^*/g$ for the residue $R = 2\kappa E/g$. We then obtain

$$g = 2E\kappa, \tag{30}$$

where E is numerically equal to the kinetic energy for $\theta_0 = 3\pi/2$, i.e., $E = V^{*2}/2$.

Similar results can be found for the elliptic billiard, where one needs to consider the curvature given by Eq. (26).

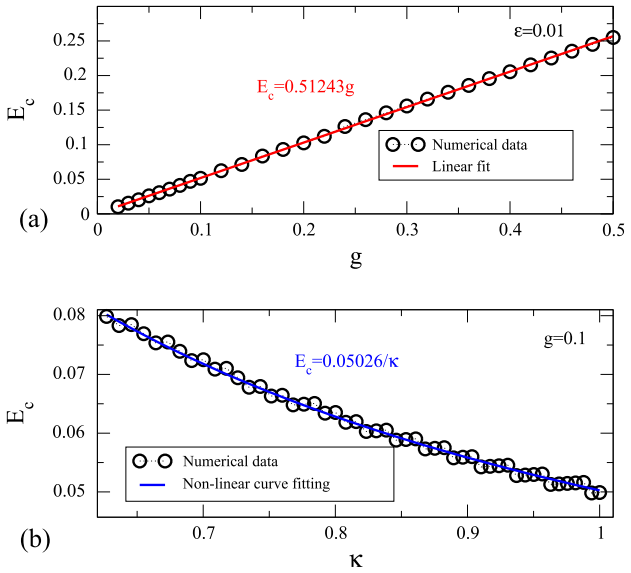

Fig. 7. For $p = 2, t_0 = 0, \theta_0 = 3\pi/2$ and $\alpha_0 = \pi/2$ we have: (a) E_c vs g for $\epsilon = 0.01$. After a linear fit, the slope obtained is 0.51243; (b) E_c vs κ considering $g = 0.1$. A non-linear curve fitting produces as result $E_c = 0.05026/\kappa$.

5. Ergodicity

In this section we test the ergodicity of the dynamics appearing in the above phase space plots, using a tool called Lyapunov weighted dynamics (LWD) to identify rare physical trajectories in the phase space [32]. Basically the method consists of considering a number of 10^4 trajectories equally distributed in the phase space. Each has a perturbed trajectory, separated by $\delta\theta_i = 10^{-3}$. Both are evolved in phase space and they are perturbed by a weak random force of intensity $\sqrt{\sigma} = 10^{-6}$ that slightly modifies the angle θ. If the particle reaches the boundary of the billiard, a new mutual separation is calculated ($\delta\theta_f$) and the separation ratio is obtained ($p_a = |\delta\theta_f|/|\delta\theta_i|$). The initial separation is renormalized by $\delta\theta_i = \delta\theta_f/p_a$. The method includes a real parameter μ, which is positive if we seek unstable dynamics, and negative otherwise. If $p_a^\mu > 1$ a clone of the trajectory and perturbation is created with a probability $p_a^\mu - 1$, otherwise the trajectory is killed with a probability $1 - p_a^\mu$. For this method, the maximum number of iterations considered are 10^3.

Fig. 8(a,b) shows a plot of the phase space (black dots) for different values of g. A period doubling bifurcation is observed for $E = 0.5, p = 2$ and $\epsilon = 0.1$ (oval billiard). For $g = 0.1$ (Fig. 8(a)) one sees the green dots ($\mu = +1$) are circulating the two large KAM islands, centering a saddle fixed point. The red dots concentrate more inside the KAM islands. Then we use $\mu = -1$ in the LWD to highlight the periodic islands. After increasing g to $g = 0.25$ (Fig. 8(b)) we see the green dots do not have a preferred region and it is clear that a period doubling bifurcation happened and the red dots follow the four big KAM islands.

Now we use LWD to show for some special combinations of parameters that KAM islands are not observed in the phase space, leading to an apparent ergodic dynamics. For the simulations we consider $g = 0.5$ and in Fig. 10(a–d) we have $\epsilon = 0$ (circle billiard), in Fig. 10(e–h) we considered $p = 2$ and $\epsilon = 0.1$ (oval billiard) and finally in Fig. 10(i–l) we have $a = 1.2$ and $b = 1$ (elliptic billiard). For $E = 0.524$ in the circle (Fig. 10(a)), $E = 0.602$ in the oval (Fig. 10(e)) or $E = 0.667$ in the ellipse (Fig. 10(i)) we observe that the trajectories and clones for the LWD are highlighting a period four KAM island. Increasing slightly more the value of E to 0.58 for the circle (Fig. 10(b)), to 0.65 for the oval (Fig. 10)) and to 0.71 for the ellipse (Fig. 10(j)) we see that the trajectories/clones are not tending to go any specific region. Possibly these regions are ergodic, but we could not prove the opposite, where several simulations were made trying to identify small KAM islands. Considering the circle with $E = 0.603$ (Fig. 10(c)), the oval billiard with $E = 0.675$ (Fig. 10)) and the elliptic billiard with $E = 0.737$ (Fig. 10(g)), we see eight KAM islands. The behavior of LWD for the billiards are not the same, and they have more complex structures with different periods that have not been shown. They have however similarities near the seemingly ergodic region. Using $E = 0.8, E = 0.73$ and $E = 0.9$, respectively for the circle, oval and ellipse, we observe again the trajectories/clones are not tending to go to any specific region.

In Fig. 11(a–c) it is shown θ as a function of E for each trajectory/clone in the circle, oval and elliptic billiard, respectively. The control parameters are labeled in the figures. For a constant value of E the periodic regions can be identified as the ones to which θ does not vary for long range.

Now we split both θ and α coordinates of the phase space in n_{div} different equally spaced regions. Therefore we have a grid with different rectangles than can be measured if are occupied by a trajectory/clone in the LWD. f corresponds to the fraction of the number of rectangles occupied over n_{div}^2. We consider in simulations $n_{div} = 1000$. Fig. 11(d–f) show f vs E for the circle, oval and elliptic billiards. We see that the apparent ergodic region has $f \cong 0.02$ for the circle and $f \cong 0.05$ for the oval and

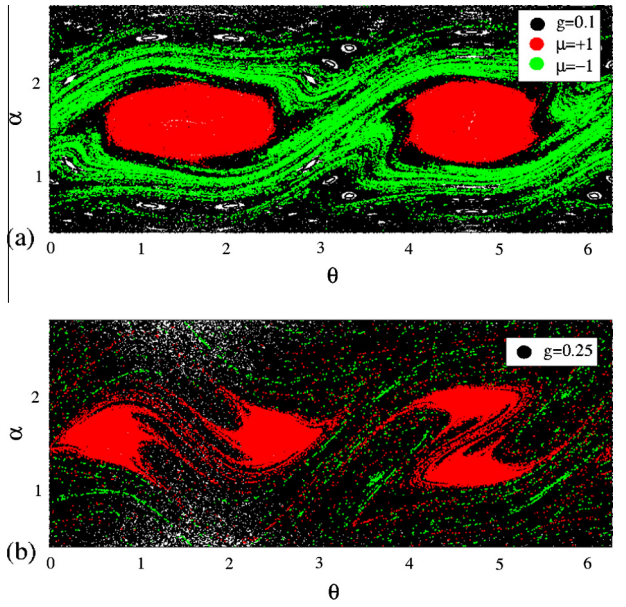

Fig. 8. Phase space (black dots) for different values of g: (a) $g = 0.1$; (b) $g = 0.25$. As red color we have the LWD considering $\mu = +1$ and in green color $\mu = -1$. We used $E = 0.5, p = 2$ and $\epsilon = 0.1$. (For interpretation of the references to color in this figure legend, the reader is referred to the web version of this article.)

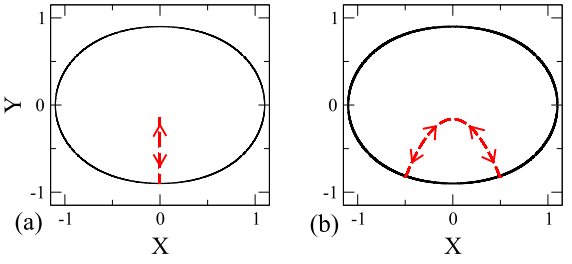

Fig. 9. An example of period one fixed point with $g = 0.5, p = 2$, $\epsilon = 0.1$ and $E = 0.38$. In (b) we have a bifurcation and the creation of a period two fixed point for $E = 0.416$. As one can see, the orbits do not reach the top for the billiard.

ellipse. The regions with periodic orbits tend to have $f \to 0$. We see for the circle (Fig. 11(d)) the ergodic and non-ergodic behaviors appear many times, as indicated by the values of E in which $f < 0.01$ for example. Therefore, figures of f vs E in other opportunities can be used as an indicative of ergodicity in a system.

5.1. Supplemental data II

As a complementary material, we have as attached files a video showing the LWD for $\mu = -1$ and considering $E \in [0.602, 0.79]$ for the circle. The Fig. 10(a–d) show some frames of this video. The video can be seen in the following electronic address http://youtube.com/watch?v=c9ybMF93JAs.

6. Time-dependent billiards

In this section we introduce a time-dependence in the boundary of the oval/circle billiard. We consider that the boundary is breathing and the radius is given by

$$R(p, \epsilon, \eta, \theta, t) = 1 + \eta \cos(t) + \epsilon[1 + \eta \cos(t)] \cos(p\theta). \tag{31}$$

For $\eta = 0$ the static boundary case is recovered. Our main purpose is to study and understand the influence of the gravitational field g in the Fermi acceleration phenomena. To do so, we define the average velocity as

$$\overline{V}(n) = \frac{1}{M} \sum_{j=1}^{M} \left[\frac{1}{n} \sum_{i=1}^{n} V_i \right], \tag{32}$$

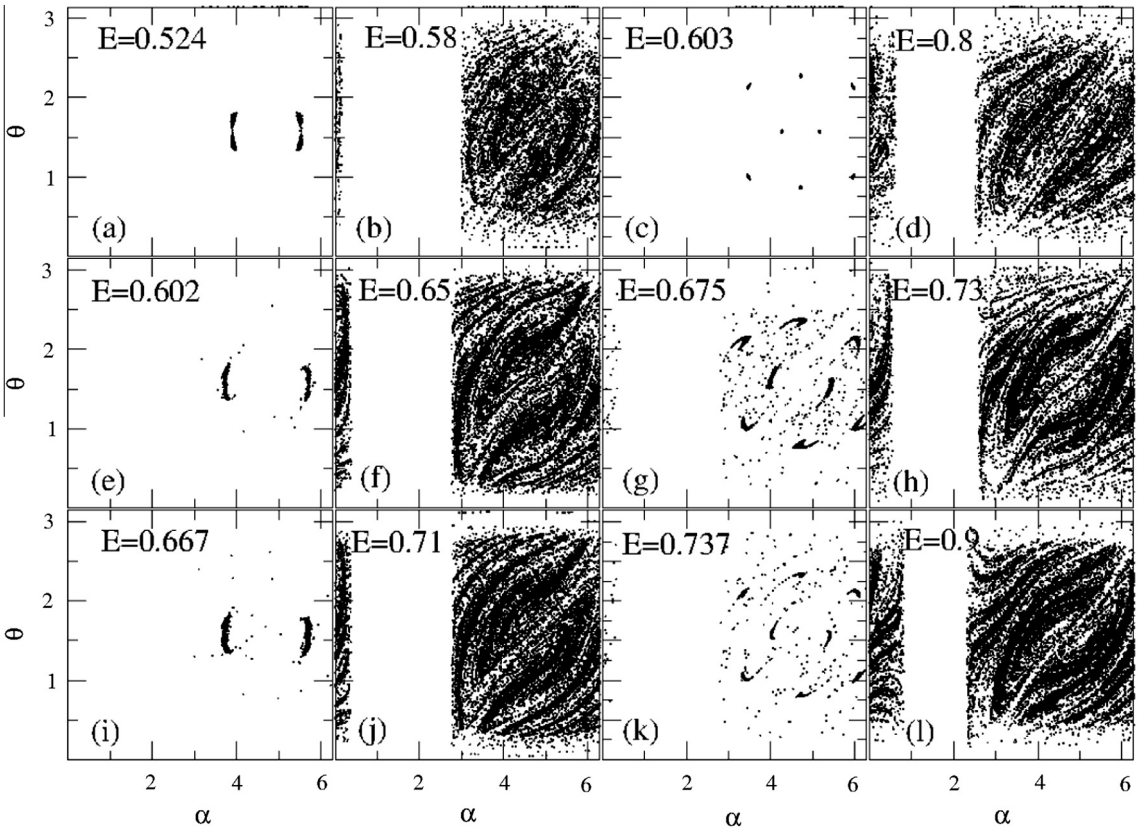

Fig. 10. For different values of E we have the position of 10^4 the trajectories and clones using the Lyapunov weighted dynamics (LWD) after 10^3 iterations and for $\mu = -1$. We have considered $\epsilon = 0$ (circle billiard) in (a)–(d). In (e)–(h) the control parameters used were $p = 2$, $\epsilon = 0.1$ and $g = 0.5$ for the oval billiard and in (i)–(l) we have considered $a = 1$ for the elliptic billiard.

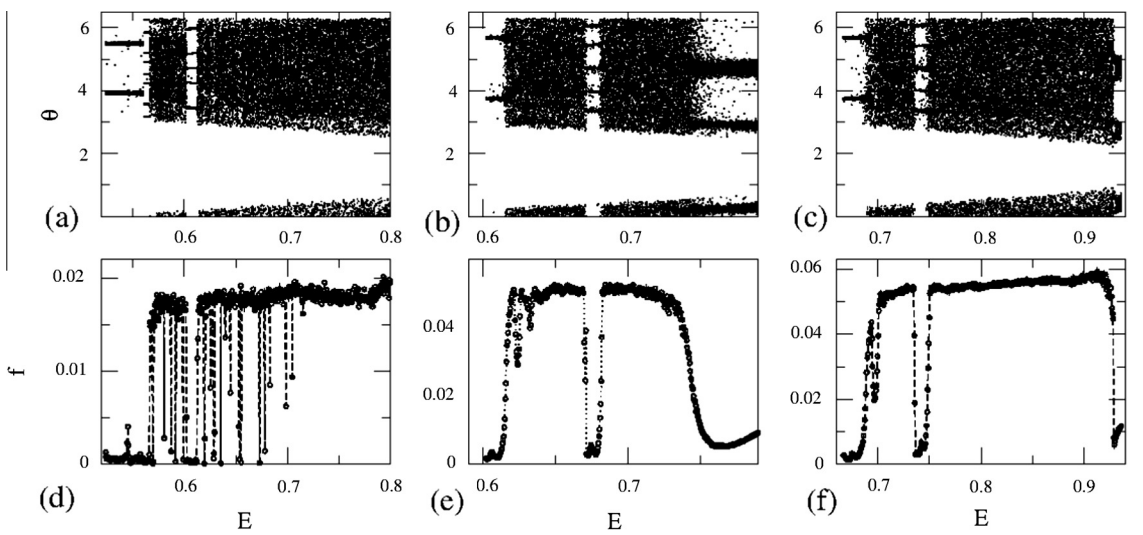

Fig. 11. For $g = 0.5$ and $\mu = -1$ we have the θ coordinate for the LWD as function of E and considering the circle in (a), oval ($p = 2$ and $\epsilon = 0.1$) in (b) and the ellipse ($b = 1$ and $a = 1.2$) in (c). In (d)–(f) we have the fraction f for the number of occupied rectangles as function of E for the circle, oval and elliptic billiard, respectively.

where $M = 500$ defines an ensemble of different initial conditions randomly chosen in $\theta_0 \in [0, 2\pi)$, $\alpha_0 \in [0, \pi)$ and $t_0 \in [0, 2\pi)$.

To discuss the results of the time dependent boundary, let us start with the case of absent gravitation field, $g = 0$. For the circle billiard, there is no chaos in the phase space for the static version. Hence initializing the simulation with a very low initial velocity, the curve of average velocity starts to grow with and then suddenly changes to a regime of saturation. Such

regime marks a final limit of grow for the velocity of the particle then no unlimited energy growth is observed. This is in well agreement to what is known in the literature, particularly the LRA conjecture.

Then let us make $g \neq 0$ but considering small values, as labeled in the figure. Because now $g \neq 0$, thin regions of the phase space for the circular case have chaos for the static boundary. The curves of average velocity seem not to saturate but rather they appear to grow at a very small rate as shown in Fig. 12(b) for a magnification considering $g = 10$. The slope of growth is 0.0209(4). Why this exponent is remarkably small? Indeed according to Arnold [42], who proved there exist solutions exhibiting arbitrarily large growth in the action variables in nearly integrable dynamical systems with several degrees of freedom. Therefore we believe few orbits are having diffusion in velocity while others are in regular dynamics that, in the average are producing the behavior shown in Fig. 12, as observed.

Now let us consider the oval billiard for $p = 2, \epsilon = 0.2, g = 0.1$ and $\eta = 0.01$. It is shown in Fig. 13(a) a plot of $\overline{V}$ as function of n for different initial velocities V_0. As one sees, the higher V_0 the higher is the initial plateau $\overline{V}$ observed until the curve changes to a regime of growth. The curves have an initial plateau with constant velocity, and after passing by a crossover n_x, they start growing with slope ∼0.1734. We notice this result is slightly larger than the one obtained [39], i.e. ∼0.16 . . . for the breathing case and foreseen theoretically in [40] as ∼1/6. However our result is within the same order of magnitude of either results obtained previously.

The simulations in Fig. 12 considered initial conditions randomly chosen. But now, we try to explain what happens with the average velocity depending on the initial condition. Fig. 14(a–c) present a grid of initial conditions (θ, α) and the color represents the value of the average velocity. In Fig. 14(a–c) we have considered the circle billiard with $g = 10$, and the number of iterations were respectively equal to $10^2, 10^4$ and 10^6. As one can see, for $0 < \theta < \pi$ the initial conditions have greater values of final average velocity when compared to the region with $\pi < \theta < 2\pi$. It happens because the initial potential energy is bigger for $0 < \theta < \pi$. Increasing the number of iterations apparently do not change this scenario. Now we consider the oval billiard with $p = 2, \epsilon = 0.2$ and $g = 0.1$, as shown in Fig. 14(d–f) for $10^2, 10^4$ and 10^6 iterations. For 10^2 iterations one can see the same scenario shown previously, where we have a clear separation between the regions $0 < \theta < \pi$ (high values of potential energy) and $\pi < \theta < 2\pi$. Increasing the number of iterations breaks down this separation, where one can see that the final average velocity is almost independent of the initial condition. But there are two distinct regions in this figure, near KAM islands that keep the average velocity as constant values. Therefore, one can conclude that the stickiness and periodic regions can affect the dynamics, mainly the diffusion in velocity.

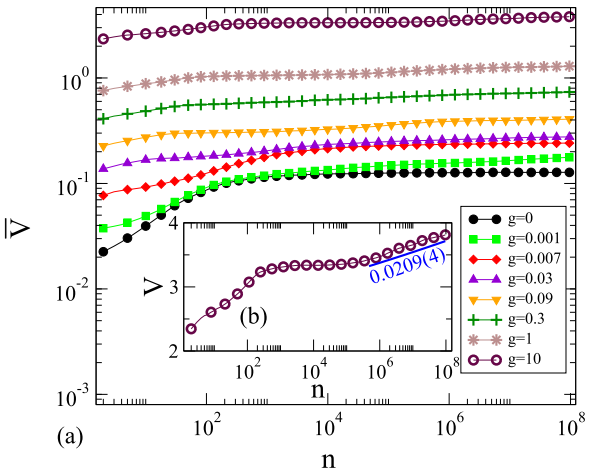

Fig. 12. For the circle billiard ($\epsilon = 0$ and $a = b$), with $V_0 = 0.01$ and $\eta = 0.01$ we have: (a) $\overline{V}$ vs n considering different values of g; (b) Magnification near the curve with $g = 10$, where it is possible to observe that the curve does not have enough time to saturate for 10^8 iterations of the mapping.

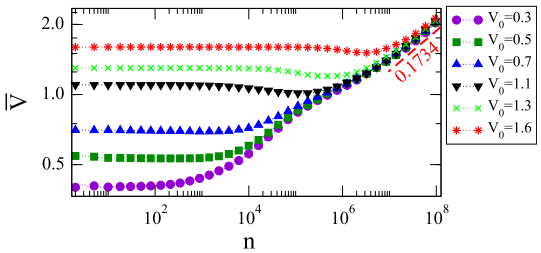

Fig. 13. For $\epsilon = 0.2, p = 2, g = 0.1$ and $\eta = 0.01$ we have $\overline{V}$ vs n considering different values of V_0.

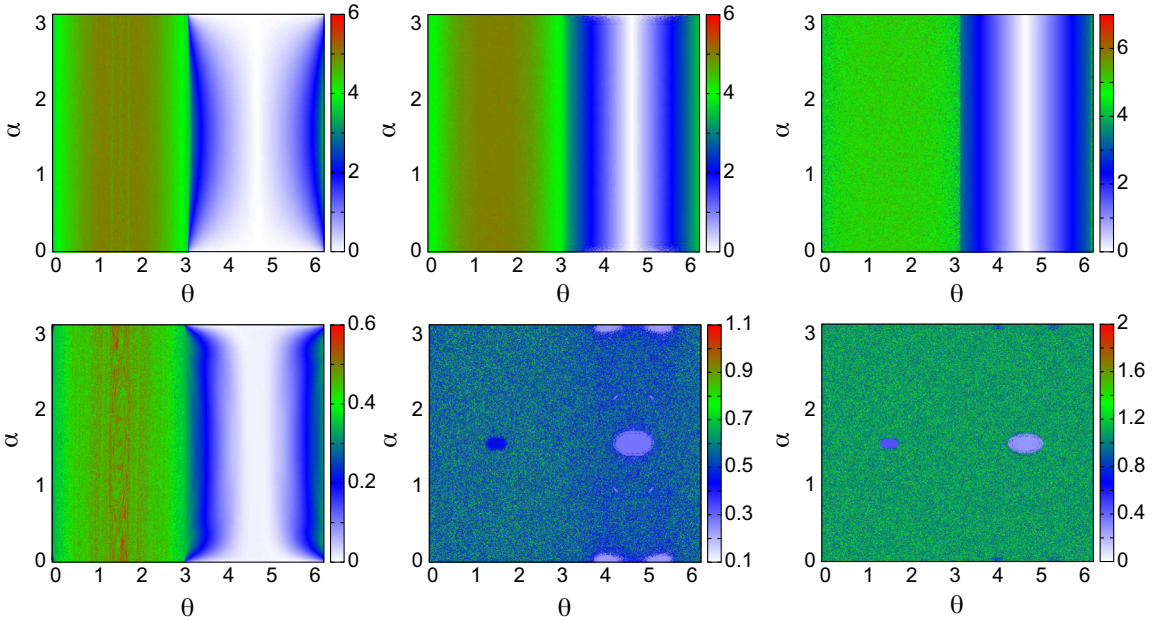

Fig. 14. In the itens (a–c) we have a circle billiard with $g = 10$ and the number of iterations are respectively equal to $10^2, 10^4$ and 10^6. The itens (d–f) consider an oval billiard ($\epsilon = 0.2, p = 2$ and $g = 0.1$) and the number of iterations are equal to $10^2, 10^4$ and 10^6, respectively. We have considered $\eta = 0.01$ to construct these figures.

As we mentioned in the Fig. 14(a,d), depending on the value of the initial angle θ, the potential energy can change, therewith increasing or decreasing the total energy of the system. For the same angle θ, apparently the choice of α does not affect the behavior of the average velocity, the only exception is near the KAM islands. Therefore, we consider now the average velocity for an ensemble of different initial condition. For this we consider a fixed value of θ and 25 different initial conditions are taken along the interval of $\alpha \in (0, \pi)$. The value of the fixed θ is chosen in the interval of $\alpha \in (0, 2\pi)$ and 25 different initial conditions are also taken. The results for the circle billiard are shown in Fig. 15(a). As one can see, there are some initial conditions that present the phenomena of Fermi acceleration, and the slopes (shown with details in Fig. 15(b)) are at the same order of magnitude as observed in the Fig. 12. Some of the initial conditions, represented by the dashed lines, tend to

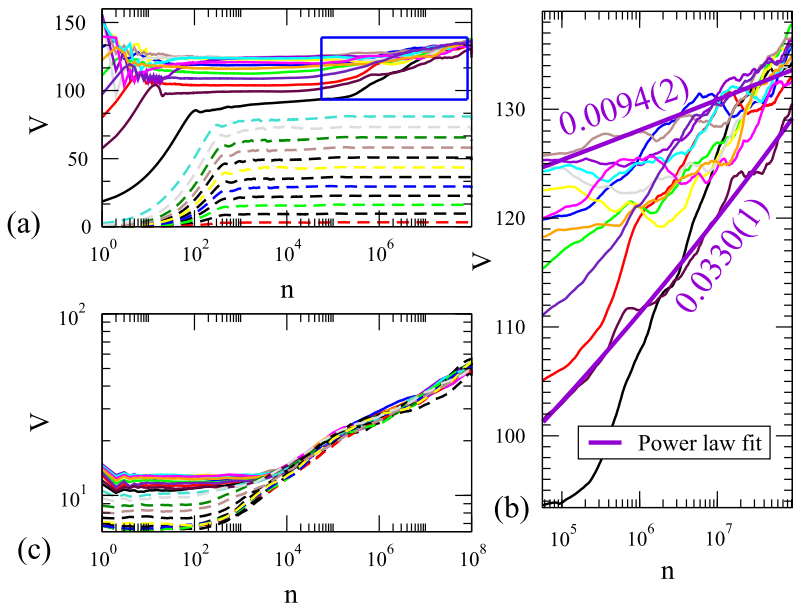

Fig. 15. Average velocity as function of n for: (a) the circle billiard with $g = 10$; (c) the oval billiard with $p = 2, \epsilon = 0.2$ and $g = 0.1$. We have considered $\eta = 0.01$.

reach a plateau of saturation after enough number of iterations. We observed that these conditions are the ones taken in the interval $\pi < \theta < 2\pi$ and they have low values of potential energy. For the oval billiard with $p = 2, \epsilon = 0.2$ and $g = 0.1$ (Fig. 15(c)), one can see that initially the orbits have a dependency on the value of θ_0, where different plateaus of constant average velocity of the ensemble are observed. After increasing the number of iterations, the curves tend to have an universal behavior with the same slopes as shown in the Fig. 13. One cannot forget there are some initial conditions influenced by periodic regions and/or stickiness, and a more detailed study must be done to study this influence.

7. Conclusions

We studied some classical particles undergoing collisions inside in a circle or oval billiard under a gravitational force field. The mapping and model were studied and details about the dynamic of these particles were realized. The linear stability of some fixed points was studied and it was possible to obtain analytically and numerically the conditions where we have a period-doubling bifurcation of a period one and two fixed points. We discovered apparently ergodic dynamics for certain values of the control parameters, which passed through a sensitive test using Lyapunov weighted dynamics. After introducing a time-dependence in the boundary, we showed for the circle with null gravity g that the system has average velocity that tends to saturate after some number of iterations n, but for $g > 0$ it is possible to see that we have a Fermi acceleration phenomenon with slope very small, where this phenomena can be explained using the LRA conjecture and Arnold diffusion. We observed that the slope for the oval billiard is slightly greater than the one obtained in the Ref. [39], but before the Fermi acceleration the particles tend to enter in a deceleration region for high enough values of initial velocity.

The numerical finding of ergodicity (strengthened by Lyapunov-weighted dynamics) for a smooth convex gravitational billiard is new; it would be interesting to obtain rigorous mathematical proofs for the examples given here, and determine conditions analogous to the defocusing mechanism for non-gravitational billiards that are sufficient for ergodicity. In addition, the dynamics of ergodic billiards is largely determined by the amount "stickiness", regular (albeit zero measure) orbits that trap trajectories for long periods. For example, the level of stickiness in the chaotic region of mushroom billiards is controlled by the existence of marginally unstable periodic orbits (MUPOs), which in turn is related to approximation of real numbers by certain rationals [7]. It would be interesting to know if the gravitational billiards considered here have dynamics controlled by similarly sticky orbits.

Likewise, we have observed Fermi acceleration in the gravitational circular billiard, despite the fact that the high velocity limit is integrable. While this is apparently due to Arnold diffusion, it would be very interesting to explore this mechanism in more detail, and in general the limit of high velocity of gravitational billiards with diverse geometries. For the oval billiard, the acceleration exponent is consistent with other (non-gravitational) Fermi acceleration problems, but this need not be the case in general. Finally, we note that both gravitational effects and time-dependent boundaries can be explored through atom-optics experiments [23].

Acknowledgments

DRC acknowledges Brazilian agency FAPESP (2013/22764-2, 2012/18962-0 and 2010/52709-5). EDL thanks to CNPq, FUNDUNESP and FAPESP (2012/23688-5), Brazilian agencies. This research was supported by resources supplied by the Center for Scientific Computing (NCC/GridUNESP) of the São Paulo State University (UNESP). This work was finished during a visit of DRC as a PhD sandwich supported by FAPESP to the School of Mathematics from the University of Bristol.

Appendix A. Supplementary data

Supplementary data associated with this article can be found, in the online version, at http://dx.doi.org/10.1016/j.cnsns.2014.08.030.

References

[1] Birkhoff GD, Dynamical systems. Providence, RI: American Mathematical Society.
[2] Dullin HR. Nonlinearity 1998;11:151–73.
[3] Courbage M, Edelman M, Saberi Fathi SM, Zaslavsky GM. Phys Rev E 2008;77:036203.
[4] Dettmann CP, Leonel ED, Available from: <arXiv:1212.5482 [nlin.CD]>.
[5] Dettmann CP. J Stat Phys 2012;146:181–204.
[6] Andreasen J, Cao H, Wiersig J, Motter AE. Phys Rev Lett 2009;103:154101.
[7] Dettmann CP, Georgiou O. J Phys A: Math Theor 2011;44:195102.
[8] Casati G, Prosen T. Phys Rev Lett 2012;109:174101.
[9] Liss J, Liebchen B, Schmelcher P. Phys Rev E 2013;87:012912.
[10] Ortega A, Stringlo K, Gorin T. Phys Rev E 2012;85:036212.
[11] Bird JP. J Phys Condens Matter 1999;11:R413.
[12] Bird JP, Akis R, Ferry DK. Phys Scr 2001;T90:50–3.
[13] Dettmann CP. Recent advances in open billiards with some open problems in Frontiers in the study of chaotic dynamical systems with open problems. In: Elhadj Z, Sprott JC, editors. World Scientific; 2011.
[14] Bunimovich LA, Dettmann CP. Phys Rev Lett 2005;94:100201.
[15] da Costa DR, Dettmann CP, Leonel ED. Phys Rev E 2011;83:066211.

[16] Fermi E. Phys Rev 1949;75:1169–74.
[17] Loskutov A, Ryabov AB, Akinshin LG. J Phys A 2000;33:7973.
[18] Berry MV. Eur J Phys 1981;2:91.
[19] Lenz F, Diakonos FK, Schmelcher P. Phys Rev Lett 2008;100:014103.
[20] Oliveira DFM, Robnik M. Phys Rev E 2011;83:026202.
[21] Leonel ED, Bunimovich LA. Phys Rev Lett 2010;104:224101.
[22] Chernov N, Dolgopyat D. J Am Math Soc 2009;22:821–58.
[23] Andersen MF, Kaplan A, Friedman N, Davidson N. J Phys B: At Mol Opt Phys 2002;35:2183–90.
[24] Hartl AE, Miller BN, Mazzoleni AP. Phys Rev E 2013;87:032901.
[25] Korsch HJ, Lang J. J Phys A: Math Gen 1991;24:45–52.
[26] Lopac V, Mrkonjić I, Radić D. Phys Rev E 2001;64:016214.
[27] Wallis H, Dalibard J, Cohen-Tannoudji C. Appl Phys B 1992;54:407–19.
[28] Livorati ALP, Kroetz T, Dettmann CP, Caldas IL, Leonel ED. Phys Rev E 2012;86:036203.
[29] Choi S, Sundaram B, Raizen MG. Phys Rev A 2010;82:033415.
[30] Szeredi T. J Stat Phys 1996;83. 1/2.
[31] Lehtihet HE, Miller BN. Physica 1986;21D:93–104.
[32] Tailleur J, Kurchan J. Nat Phys 2007;3:203–7.
[33] Tanase-Nicola S, Kurchan J. J Stat Phys 2004;116:1201–45.
[34] Tailleur J, Tanase-Nicola S, Kurchan J. J Stat Phys 2006;122:557–95.
[35] Tanase-Nicola S, Kurchan J. Phys Rev Lett 2003;91:188302.
[36] Geiger P, Dellago C. Chem Phys 2010;375:309–15.
[37] Lazutkin VF. Math USSR Izv 1973;7:185–214.
[38] Grigo A, Billiards and statistical mechanics (thesis), Georgia Tech.; 2009, <http://hdl.handle.net/1853/29610>.
[39] Leonel ED, Oliveira DFM, Loskutov A. Chaos 2009;19:033142.
[40] Batistic B, Robnik M. J Phys A: Math Theor 2011;44:365101.
[41] Oliveira DFM, Leonel ED. Commun Nonlinear Sci Numer Simul 2010;15:1092.
[42] Arnold VI. Soviet Math Dokl 1964;5:581–5.